Ab initio characterization of transition-metal-doped Si nanocrystals

R. Leitsmann,* C. Panse, F. Küwen,† and F. Bechstedt
European Theoretical Spectroscopy Facility (ETSF)
and Institut für Festkörpertheorie und -optik, Friedrich-Schiller-Universität Jena, Max-Wien-Platz 1, 07743 Jena, Germany
(Received 23 June 2009; revised manuscript received 13 August 2009; published 11 September 2009)

We investigate the influence of transition-metal doping on silicon nanocrystals by means of first-principles calculations within a supercell approach. We focus on the energetic stability of different doping sites and on electronic and magnetic properties of the most stable configurations. Remarkable differences concerning the magnetic moments and the electronic properties are found between iron and manganese and for inclusion of strong electron correlation. In addition, a self-purification effect, which hampers an incorporation of transition-metal atoms in small nanocrystals, is observed.

DOI: 10.1103/PhysRevB.80.104412 PACS number(s): 61.72.−y, 68.55.Ln, 73.22.−f, 75.50.Pp

I. INTRODUCTION

In the last years there has been a growing interest in diluted magnetic semiconductors. The resulting spin-dependent properties allow us to study novel transport effects and to construct novel spintronic devices.[1] For industrial applications, however, spintronics must conquer silicon, the abundant, inexpensive, and entrenched material of choice for conventional semiconductor electronics.[2] One way could be alloying or doping silicon with transition-metal (TM) atoms such as Mn or Fe.[3] In addition, the discovery of an increasing number of spin-related effects shows that the spin of electrons offers unique posibilities for novel mechanisms of information processing.[4,5] Possible new devices can be "spin-effect transistors" or "spin qubits."[6]

The chemical trends of the TM doping of bulk Si and its influence on electronic energy levels have been studied theoretically by self-consistent methods over the years in detail.[7–10] However, quantum confinement of electrons greatly alters various properties of materials. This has been demonstrated for semiconductor nanocrystals (NCs) under several aspects.[11] For spin and magnetic properties most notably is the unusual increase in spin-dephasing time.[4] In the current focus of theoretical and experimental studies there are Mn-doped II–VI and III–V semiconductors but also Ge nanocrystals.[11–16] TM doping of Si nanostructures becomes also interesting, as recently shown for Si nanowires.[17] Those quasi-one-dimensional structures exhibit an half-metallic character under certain conditions. Room-temperature ferromagnetism seems to be discovered for Mn^+-doped Si nanowires.[18] However, a detailed understanding of the formation of ferromagnetism due to TM incorporation on the nanometer scale requires a much deeper analysis of the TM doping of silicon for various nanostructure sizes, dopants, and doping sites. This concerns the formation energy as a function of the impurity position and the defect-induced electronic structure. Another open question concerns the influence of the electronic correlation especially within the localized semicore TM 3*d* states on the defect-level positions, their occupation, and the accompanying magnetic moments.[19–21]

In the present paper the effect of TM doping on Si nanostructures is studied for the model systems of hydrogen-passivated Si NCs. More in detail, the incorporation of Mn and Fe atoms into Si NCs is investigated in the framework of the spin-polarized density-functional theory (DFT). Special attention is paid on the stability of the NC structures with respect to the different doping sites and NC diameters. In addition we study possible self-purification effects and the influence of the TM 3*d*-derived impurity states on the electronic and magnetic properties. Furthermore, we take into account strong electron-correlation effects via a Hubbard-type Coloumb repulsion U.[22]

II. MODELING AND METHODS

A. Nanocrystal construction

The Si NCs are modeled using a supercell method,[23] i.e., periodic boundary conditions are applied. We use a simple cubic arrangement of the supercells. Each of them contains one NC and a certain amount of vacuum. The size of the simple cubic supercells varies with the diameter of the NCs and the extent of the vacuum region. The chosen edge lengths guarantee a distance larger than 1 nm between the surfaces of the NCs in adjacent supercells. In addition, we restrict the studies to NCs with one incorporated atom. The atomic positions are determined by a shell-by-shell construction, successively adding Si atoms in a local tetrahedron coordination and a subsequent structural optimization. For the passivation of the surface dangling bonds hydrogen atoms are used. With this procedure we obtain NCs with varying total number of shells $N=2$, 3, 4, 5, and 6 and corresponding diameters $D=0.6$, 1.0, 1.4, 1.8, and 2.2 nm (cf. Fig. 1 and Table I). They possess 5, 17, 41, 83, and 147 Si atoms. Together with the hydrogen passivation the described procedure yields Si_5H_{12}, $Si_{17}H_{36}$, $Si_{41}H_{60}$, $Si_{83}H_{108}$, and $Si_{147}H_{148}$ NCs. A detailed description of the construction of pure Si NCs can be found elsewhere.[24,25]

Each constructed NC contains six rectangular {001} and eight triangular {111} surface facets (Fig. 1). We consider only doping situations with one TM atom per NC. The possible doping positions are marked either with red (substitutional) or with blue (interstitial) atoms. In contrast to Si bulk crystals, the doping properties depend on the TM-atom position in the NC with respect to the NC center and the NC

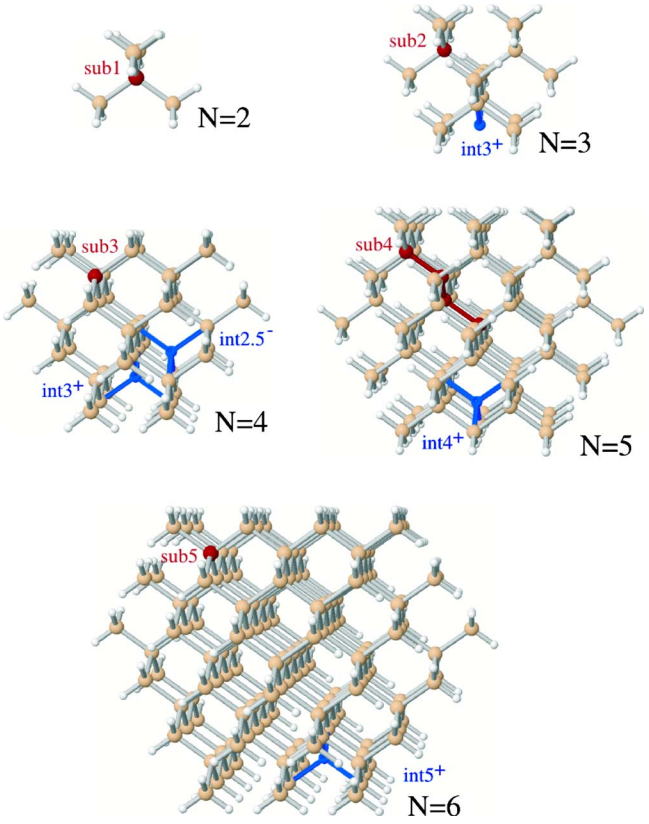

FIG. 1. (Color online) Schematic stick-and-ball representation of the used Si NCs. The positions of different substitutional and interstitial doping sites are indicated.

surface. Thereby, one has to take into account the existence of different surface facets and edges in between. To distinguish between doping positions with different symmetries we introduce the following notation: (type $n)^i$ with $i \in \{+, -\}$. The *type* can be either "sub" or "int" for a substitutional or an interstitial position, respectively. The radial position inside the NC is indicated by the shell number $n \leq N$, where $n=1$ denotes the position in the NC center. In some cases this number is an integer (dopant in one Si shell). However, in other cases the dopant occupies a side between two Si shells. Therefore, in this case "n" is replaced by the averaged shell number, i.e., by a half-integer value. The index i denotes the position of the dopant with respect to the type of the surface facet. Dopants under a rectangular facet are indicated by "+" and dopants under triangular facets by "−."

Since all NCs are doped with one TM atom, different dot sizes lead to different doping concentrations (see Table I). The point group of a TM-doped Si crystal is only a subgroup of the T_d symmetry of bulk Si and undoped Si NCs. Nevertheless, we still approximatively classify the TM 3*d* states in terms of e_g- and t_{2g}-orbital symmetries. The reliability of this procedure will be discussed in Sec. III B in detail.

B. Total-energy calculations

In order to investigate clean and doped silicon nanocrystals by first-principles techniques we use the spin-polarized DFT as it is implemented in the Vienna *ab initio* simulation package (VASP).[26] The pseudopotentials are generated by means of the projector-augmented-wave method[27] that allows an accurate treatment of the TM 3*d*, TM 4*s*, Si 3*s*, and Si 3*p* valence electrons. In the region between the atomic cores the wave functions are expanded in-plane waves up to a cutoff energy of 200 eV. To approximate the exchange and correlation (XC) functional we use the generalized gradient approximation (GGA) as parametrized by Perdew and Wang.[28,29] For intermediate spin polarizations we apply the interpolation proposed by von Barth and Hedin.[30] Since we are using huge supercells, it is reasonable to restrict the reciprocal-space summation to the Γ point. The atomic geometries are optimized within the GGA approach until the corresponding Hellmann-Feynman forces are smaller than 25 meV/Å. The approach has been tested for Mn doping of bulk Si. Good agreement with other recent first-principles calculations[31–33] was found, at least with respect to the geometric properties.

The eigenvalues of the accompanying Kohn-Sham (KS) equation are used to discuss the electronic structure, especially the density of states (DOS). The corresponding eigenfunctions for the occupied states lead to the magnetization density $m(\boldsymbol{x})=\mu_B[n_\uparrow(\boldsymbol{x})-n_\downarrow(\boldsymbol{x})]$, defined as the difference of majority-spin and minority-spin densities $n_\uparrow(\boldsymbol{x})$ and $n_\downarrow(\boldsymbol{x})$, respectively (Fig. 2). Because of the lack of excitation aspect in the DFT ground-state theory the KS eigenvalues lead to too small energetic distances between occupied and empty states. The fundamental energy gap of bulk Si $E_g=0.67$ eV underestimates, therefore, the experimental gap by about 05. eV. This underestimation can be lifted within a quasiparticle picture.[34] However, since we are interested in a description of Si NCs with strong electron confinement such corrections are neglected.[24,25] The use of a quasiparticle description is

TABLE I. Doping concentration and NC diameter of the investigated Si NC structures. In addition, the average distance $d_{\text{Si-TM}}$ of the doping TM atom to it's four Si neighbors is also listed.

Number of shells N		2	3	4	5	6
Diameter (Å)		6.3	10.4	14.3	18.2	21.8
Dopant	sub	25	6.25	2.50	1.22	0.68
Concentration (%)	int		5.88	2.44	1.20	0.68
$d_{\text{Si-Mn}}$ (Å)	(sub $N-1$)	2.34	2.39	2.46	2.46	2.49
	(int $N-1)^+$			2.61	2.61	2.62
$d_{\text{Si-Fe}}$ (Å)	(sub $N-1$)	2.26	2.33	2.42	2.43	2.46
	(int $N-1)^+$			2.55	2.55	2.60

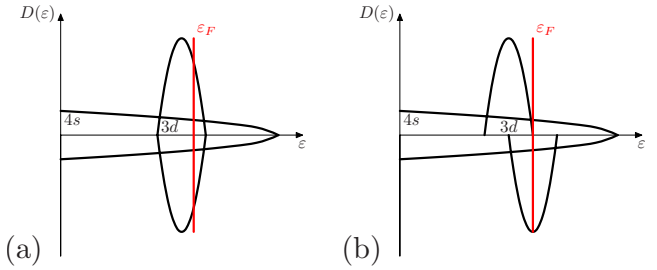

FIG. 2. (Color online) Schematic illustration of the influence of a Hubbard-type Coulomb repulsion U on the DOS: (a) $U \approx 0$ and (b) $U > 0$. Both majority- and minority-spin channel DOS are indicated.

too computer-time consuming and leads not really to novel insights into the magnetic and electronic properties. The relative positions of the TM impurity-derived electronic states in the fundamental Si gap allows the discussion of trends with respect to the influence of impurity site, NC size, and chemical nature of the impurity.

C. Approaches beyond GGA

As recently discussed in the literature[19,35,36] TM atoms experience a strong on-site Coulomb repulsion U among their $3d$ electrons due to the narrow d bandwidth, which is not correctly described in a spin-polarized DFT treatment. This error can be corrected with the DFT+U method, which is a combination of the DFT and a Hubbard-type description of the Coulomb repulsion in the Hamiltonian. Since the strength of the on-site repulsion is proportional to localization of the corresponding wave functions, it has to be considered only in the case of strongly localized TM $3d$ states. For the present calculations we use a simple DFT+U version, proposed by Dudarev *et al.* in Ref. 36. The spin-dependent interaction leads to a difference in the band energies between majority- and minority-spin channel

$$\varepsilon_{3d,\uparrow} - \varepsilon_{3d,\downarrow} = \Delta = U(n_{3d,\downarrow} - n_{3d,\uparrow}), \tag{1}$$

where we have introduced the exchange splitting Δ and the partial occupation numbers of the TM $3d$ states, $n_{3d,\uparrow}$ and $n_{3d,\downarrow}$. The differences [Eq. (1)] in the band energies may have considerable consequences on the electronic properties of the investigated TM-doped Si NCs and will, therefore, be included in our calculations within the GGA+U approach. To obtain the correct band ordering the Hubbard-type Coulomb repulsion U is limited to a value of 3 eV as proposed in Ref. 37. This value leads to the correct energetic ordering of the valence and conduction bands, at least for antiferromagnetic MnO. More sophisticated methods such as the spatially nonlocal hybrid functional HSE03 yield qualitatively the same results as a GGA+U treatment,[19] apart from a splitting of partially filled impurity states. Since the applications of hybrid functionals are very computer-time consuming, especially for larger NCs and low-symmetry doping sites, they will not be considered in this study.

III. RESULTS AND DISCUSSION

A. Stability and geometry

We first study the energetic stability of the TM-atom incorporation on a substitutional or interstitial site in a certain radial distance to the NC center. To allow a discussion of different preparation conditions Plancks's grand canonical thermodynamic potential has to be studied for a given doped Si NCs with $N_{\mathrm{Si:TM}}$ Si atoms and N_{TM} TM atoms. Thereby, the actual chemical potentials μ_{Si} and μ_{TM} of the reservoirs of Si and TM atoms, characterize the preparation conditions. More precisely, we calculate the formation energy of a doped NC as

$$\Omega_f = \gamma_f - \mu_{\mathrm{TM}} N_{\mathrm{TM}} \tag{2}$$

with

$$\gamma_f = E_{\mathrm{tot}}^{\mathrm{Si:TM}} - E_{\mathrm{tot}}^{\mathrm{Si}} - \mu_{\mathrm{Si}}(N_{\mathrm{Si:TM}} - N_{\mathrm{Si}}), \tag{3}$$

where $E_{\mathrm{tot}}^{\mathrm{Si:TM}}$ is the total energy of the doped NC, $E_{\mathrm{tot}}^{\mathrm{Si}}$ is the total energy of the undoped NC with N_{Si} Si atoms, and μ_X (X=Si,TM) are the chemical potentials of the two species. With the chemical potential of bulk silicon $\mu_{\mathrm{Si}}^{\mathrm{bulk}}$ the relative formation energy γ_f [Eq. (2)] can be studied as a function of the variation in the Si chemical potential $\Delta\mu_{\mathrm{Si}} = \mu_{\mathrm{Si}} - \mu_{\mathrm{Si}}^{\mathrm{bulk}}$. The relative formation energy γ_f is sufficient since we compare the formation energies of different nano-objects with a fixed number $N_{\mathrm{TM}}=1$ of TM dopants. The bulk chemical potential $\mu_{\mathrm{Si}}^{\mathrm{bulk}}$ is computed as negative cohesive energy. The variation $\Delta\mu_{\mathrm{Si}}$ allows us to vary between Si-rich ($\Delta\mu_{\mathrm{Si}}=0$) and Si-poor ($\Delta\mu_{\mathrm{Si}} \to -\infty$) preparation conditions, at least for preparation under conditions close to thermal equilibrium. The relative formation energy γ_f is, therefore, appropriate to discuss the relative stability of different doping positions and different numbers $N_{\mathrm{Si:TM}}$ in a NC with a certain size.

The *ab initio* calculated formation energies are graphically represented in Fig. 3. For two selected H-passivated Si NCs, $Si_{41}H_{60}$ and $Si_{147}H_{148}$, and the two different TM dopants, Mn and Fe, γ_f is plotted versus the variation $\Delta\mu_{\mathrm{Si}}$ in the actual Si chemical potential. The γ_f curves for interstitial positions remain constant while such for substitutional positions vary linearly with $\Delta\mu_{\mathrm{Si}}$. As expected from bulk results,[31–33] the interstitial TM positions are more stable under Si-rich conditions while the substitutional TM positions are preferred for Si-poor conditions. This holds for all NCs with a diameter larger than 7 Å. For smaller NCs with $N=2$ the definition of interstitial doping sites is difficult. In addition, the range of the chemical potential, for which substitutional or interstitial sites are preferred, depends on the radial distance from the NC center.

Beside this general trend two different effects are visible in Fig. 3. First, under Si-poor conditions we find that the doping site directly beneath the NC edges (sub $N-1$) is always the most stable one. However, in this case three different structural configurations very close to energy appear. They will be indicated by the subscripts $\{s,m,i\}$. In the first one $(\mathrm{sub}\ N-1)_{\mathrm{s}}$ only small lattice distortions can be obtained. In the second case $(\mathrm{sub}\ N-1)_{\mathrm{m}}$ the TM atom together with the Si corner atom moves inside a neighboring zb cage[38] toward an interstitial site. However, in contrast to the

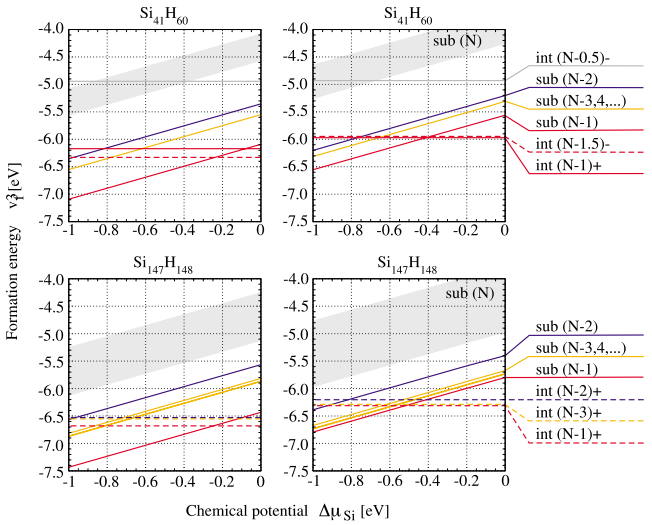

FIG. 3. (Color online) Relative formation energy of differently sized NCs with incorporation of one Mn (left panel) or Fe (right panel) atom versus the variation in the Si chemical potential $\Delta\mu_{\mathrm{Si}}$ with respect to its bulk value. The corresponding doping sites are indicated.

third case $(\text{sub } N-1)_{\mathrm{i}}$, where the TM atom reaches an interstitial position and the Si corner atom closes the *zb* cage, the $(\text{sub } N-1)^{c}_{\mathrm{m}}$ TM atom retains at an intermediate position. The configurations $(\text{sub } N-1)_{\mathrm{m}}$ and $(\text{sub } N-1)_{\mathrm{i}}$ are the most stable ones with formation-energy differences <40 meV(Mn) or <140 meV(Fe) but they are separated by an energy barrier of about 200 meVas can be seen in Fig. 4. Therefore, in room-temperature experiments both configuration types may appear. The first configuration $(\text{sub } N-1)_{\mathrm{s}}$ is only stable for Mn dopants. In the case of Fe doping no energy barrier to $(\text{sub } N-1)_{\mathrm{m}}$ appears.

Second, at Si-rich conditions we find a preference of interstitial doping sites directly beneath the rectangular {001} NC-surface facets $(\text{int } N-1)^{+}$. This result can be understood by simple geometric arguments. Due to a symmetry reduction we find an increase in the formation energy from the NC center to the surface of the NC. On the other hand, directly beneath the NC surface it is easier to distort the (incomplete)

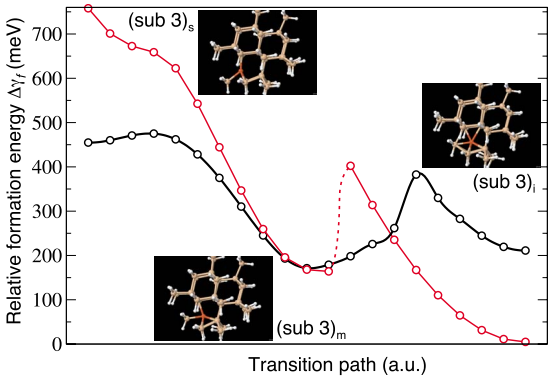

FIG. 4. (Color online) Energy barriers between the three subsurface doping positions in a $Si_{40}TMH_{60}$ NC: black for Mn dopants and red (dark gray) for Fe dopants. The insets show stick-and-ball models of the corresponding NC geometries.

tetrahedron bonding configuration of the Si atoms to incorporate a TM atom. The combination of both effects gives rise to the observed behavior. Similar results concerning the stability of different doping sites have been reported for P-doped Si NCs.[39–42]

The local distortions around the incorporated TM atoms depend on NC and doping parameters. In undoped Si NCs the Si-Si bond length depends on the radial position of the Si atoms inside the NC. We observe in agreement with the literature[43] in the center (at the surface) of the NC a slightly increased (reduced) Si-Si bond length in comparison to Si bulk, resulting in a tensile (compressive) strain. A more detailed investigation of the structural properties of undoped Si NCs can be found in Ref. 24. The incorporation of TM atoms leads to a local distortion of the Si-Si bonding configuration. Most characteristic are the distances of the TM dopant to its four Si neighbors. Thereby, the resulting averaged Si-TM bond length $d_{\text{Si-TM}}$ depends on radial position, the type of the TM atom, and on the size of the NCs. In Table. I the values for $(\text{sub } N-1)$ and $(\text{int } N-1)^{+}$ doping sites are listed as examples. Since the tetrahedral configuration of the Si atoms around interstitial doping sites can hardly be disturbed due to the weak bonding, the corresponding lengths $d_{\text{Si-TM}}$ are always larger than for substitutional doping sites. In comparison to results for TM incorporation in bulk silicon[31,32] the TM-Si distances in the $(N-1)$ shell of a NC with N shells are always larger than the corresponding bulk values. Additionally there is a clear tendency of an increase in the TM-Si neighbor distances with the radial distance of the defect to the NC center. Thereby, this effect is more pronounced for Mn than for Fe incorporation.

In order to study the influence of the NC size on the TM defect formation we discuss the relative formation energy $\Delta\gamma_f$ of TM incorporation with respect to the formation energy of the corresponding bulk material[13]

$$\Delta\gamma_f = \gamma_f - \gamma_f^{\text{bulk}}. \tag{4}$$

Here γ_f is the relative formation energy of TM defects in Si nanocrystals as defined in Eq. (3) while γ_f^{bulk} refers to the relative formation energy in an infinitely large NC, i.e., of the corresponding bulk material. We describe γ_f^{bulk} by that of a Si crystal with a doping concentration of about 0.5%. Details of this calculations have been published elsewhere.[31] For the most stable doping sites the results are plotted in Fig. 5 for different NC sizes. With decreasing NC size the relative formation energy $\Delta\gamma_f$ increases, which means that the incorporation of TM atoms is hampered (at least for preparation conditions close to the thermodynamic equilibrium). This is a consequence of the increased doping concentration in small NCs. However, the change in the relative formation energy with increasing doping concentration in bulk Si is much smaller than the effect shown here. Therefore, together with the most stable sites for TM incorporation in subsurface positions, we interprete Fig. 5 as a clear evidence for the so-called self-purification effect proposed for several nanostructures in the literature.[11,13,16,39] This effect is more pronounced for Fe impurities. Consequently, based on our DFT-GGA calculations, one may conclude that Mn atoms can be incorporated in NCs more easily than Fe atoms.

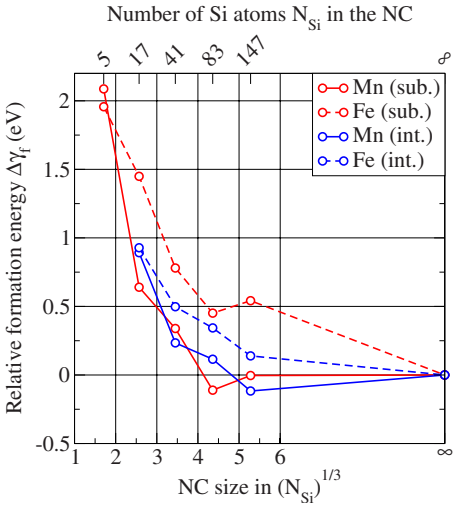

FIG. 5. (Color online) Relative formation energy $\Delta\gamma_f$ for the most stable substitutional (red) and interstitial (blue) doping sites. Solid lines illustrate the incorporation of Mn atoms and dashed lines Fe atoms.

B. Electronic structure and magnetic properties: General picture

Before we present the electronic-structure results of the *ab initio* calculations we first consider a simple defect-molecule model, as shown in Fig. 6. The neighboring Si sp^3 hybrid orbitals pointing toward a substitutional impurity with almost conserved T_d symmetry split into the nondegenerate a_1 state and the threefold degenerate t_{2g} states, which form molecular bonds with the $3d$ t_{2g} states and the $4s$ states of the

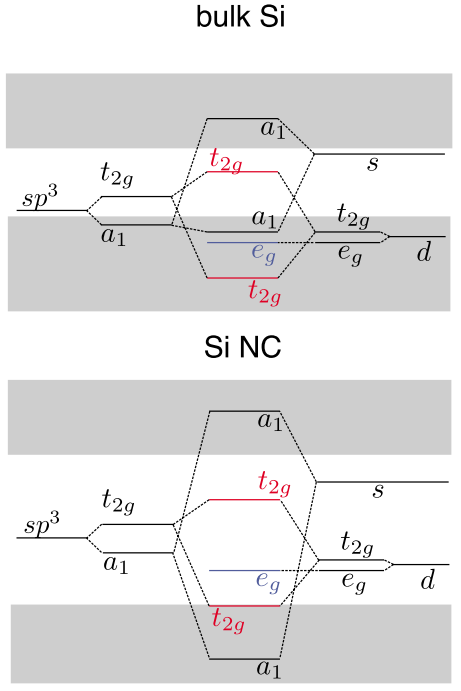

FIG. 6. (Color online) Energy-level diagram of a simple defect-molecule model with T_d symmetry. The shaded regions correspond to Si states of the undoped system.

TM impurity. The resulting bonding (antibonding) a_1 states appear in the energy region of the valence (conduction) bands of the pure Si system while the TM $3d$-derived nonbonding e_g states are mainly localized in the fundamental gap region. Due to their bonding or antibonding character and the energy differences between Si sp^3 hybrids and TM $3d$ states, the t_{2g} molecule states have either dominant TM $3d$ or Si sp^3 character. Consequently, the antibonding t_{2g} molecule levels may appear in the fundamental gap of bulk Si (see Fig. 6, left panel) whereas the position of the bonding t_{2g} level with respect to the band edge depends on the confinement. In Si NC systems the confinement effect leads to a widening of the fundamental band-gap region. Nevertheless, the a_1 molecule levels always appear in the energy regions of the empty and occupied Si NC levels due to the increased bonding-antibonding splitting of the states compared to the bulk Si situation. The defect-derived t_{2g} and e_g levels may now occur in the gap between the lowest-unoccupied nanocrystal orbital (LUNO) and the highest-occupied nanocrystal orbital (HONO) of the undoped Si NC (see Fig. 6, right panel). Such a simple defect-molecule model can already explain many features (especially the magnetic moment) within the empirical model introduced by Ludwig and Woodbury[44] for TM point defects in bulk silicon.[31]

The *ab initio* calculated electronic structures due to the impurity incorporation in Si NCs are described by energy-level diagrams in Figs. 7–11 for different NC sizes and doping sites. Figures 7 and 8 show the influence of the distance to the NC center while Figs. 9 and 10 indicate the influence of different subsurface doping positions. The dependence of the impurity states on the NC size is illustrated in Fig. 11. The energy regions of occupied and empty electronic states in undoped Si NCs are indicated by shaded regions. The alignment of the energy scales of doped and undoped situtations has been made by means of the electrostatic potentials occurring in the KS equation. The corresponding shifts ΔV are, however, unworthy small. Only for Fe they exceed values of about 0.04 eV. The vacuum level is chosen as energy zero.

In agreement with the defect-molecule model (Fig. 6), in Figs. 7–11 TM $3d$ states with e_g and t_{2g} character appear within the fundamental gap. However, beyond the simple model one has to take into account that [apart from (sub 1) impurities] the T_d symmetry of the undoped Si NCs is disturbed. This symmetry reduction explains why e_g- and t_{2g}-derived levels in Figs. 7 and 8 are usually splitted. Their twofold or threefold degeneracy is fully (e_g) or partially (t_{2g}) lifted. These splittings increase with increasing distance of the doping position from the NC center. The largest (nano)crystal-field splittings occurs close to the NC surface. In the case of subsurface doping sites the structural changes become so large that one cannot speak about a distorted T_d symmetry anymore. Nevertheless, if possible we will keep the T_d-symmetry-based notation of the impurity states with e_g and t_{2g} in order to visualize their origin. For all impurity states the degeneracy is almost lifted. On the other hand the center of gravity of the levels derived from the same symmetry is less influenced by the radial position of the incorporated TM atom.

The observed general behavior holds for both XC functionals GGA and GGA+U and both dopants Fe and Mn.

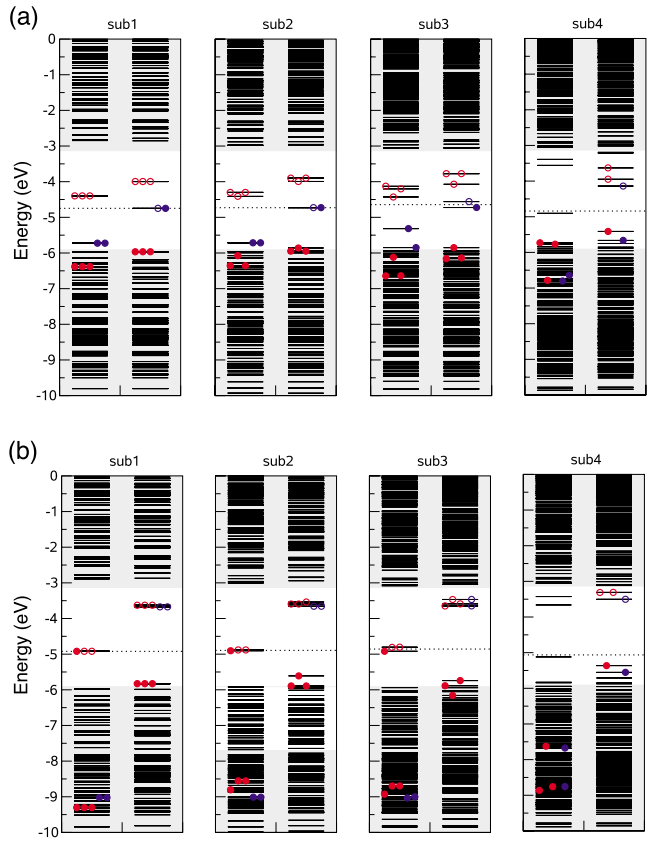

FIG. 7. (Color online) Energy-level diagrams of a $Si_{82}MnH_{108}$ NC with $N=5$ for substitutional doping sites at different radial positions. The gray regions correspond to conduction and valence states of the bare (undoped) Si NCs. The horizontal black lines represent the energy levels of the doped Si NCs. The degeneracy of the TM $3d$ states (e_g—blue and t_{2g}—red) is illustrated by open (empty) and filled (occupied) circles. Results in (a) GGA and (b) GGA+U ($U=3$ eV) are presented. The horizontal dotted line defines the Fermi level. Majority-spin (left) and minority-spin (right) channels are shown.

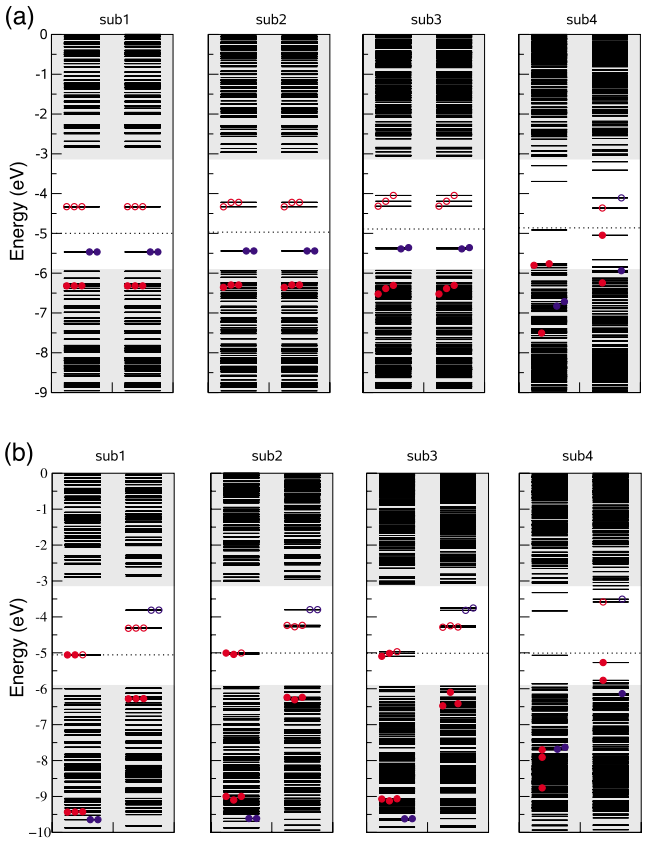

FIG. 8. (Color online) As in Fig. 7 but Fe instead of Mn.

However, the bonding (antibonding) TM $3d$-derived states are located at much lower (higher) energies in the GGA+U case. This leads to a spin flip of electrons, which is accompanied by the transfer of one electron from the minority-spin channel into the majority-spin channel. Hence a change in the total magnetic moment from a low-spin phase $\mu_{\text{tot}}=1\mu_B$ (GGA, Mn), $\mu_{\text{tot}}=0\mu_B$ (GGA, Fe) to a high-spin phase $\mu_{\text{tot}}=3\mu_B$ (GGA+U, Mn), $\mu_{\text{tot}}=4\mu_B$ (GGA+U, Fe) occurs. Only in the case of subsurface doping sites the crystal-field splitting is so large that one observes a high-spin phase for Mn dopants or a mediate-spin phase ($\mu_{\text{tot}}=2\mu_B$) for Fe dopants already in the GGA approach. In this case, one of the antibonding t_{2g} levels in the minority-spin channel is shifted below the Fermi level so that a spin flip occurs and the magnetic moment of the NC changes. Furthermore, at subsurface doping sites the antibonding t_{2g} levels of the majority-spin channel and the bonding t_{2g} levels of the minority-spin channel loose their tetrahedral symmetry character completely so that we cannot indicate them anymore in the corresponding energy-level diagrams. The appearance of the mediate-spin phase for Fe dopants near the NC surface can be understood by taking the actual geometry into account. The substitutional subsurface doping sites have at least a partially interstitial-like character. For interstitial doping sites in bulk Si, however, it has been shown that Fe dopants yield in both XC approximations, GGA and GGA+U, a total magnetic moment of $2\mu_B$.[31] The lift of the degeneracy due to the symmetry break suggests an insulating character of all TM-doped Si NCs, also for TM=Mn with an odd number of electrons. This is in contrast to the theoretical findings for Si nanowires with adsorbed TM atoms[17] but in agreement with the strong ionic relaxation after impurity incorporation. However, the smallest Mn-doped NCs or central doping sites exhibit still a half-metallic character. This is a consequence of the almost complete degeneracy of the impurity levels within the fundamental gap region. The reason for their half-metallic character is the partial occupancy of the degenerate e_g GGA or t_{2g} (GGA+U) level. Only XC functionals with at least partial incorporation of the Fock operator (such as, e.g., HSE03) and an asymmetric level occupation give rise to a lift of this degeneracy.[19]

C. Electronic and magnetic properties of subsurface doping sites

Since for the most stable substitutional subsurface doping sites three different geometries $(\text{sub } 3)_s$, $(\text{sub } 3)_m$, and $(\text{sub } 3)_i$ appear, we compare the electronic properties of these structures in Figs. 9 and 10. While the doping sites $(\text{sub } 3)_s$ and $(\text{sub } 3)_m$ exhibit an high-spin (Mn) or mediate-

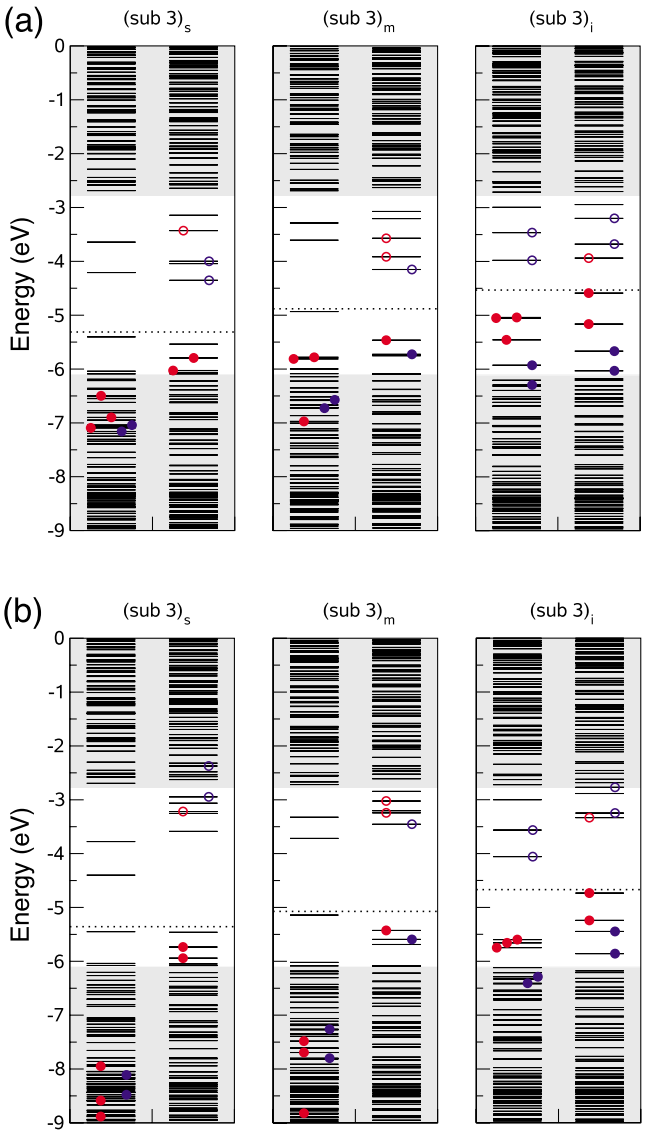

FIG. 9. (Color online) Energy-level diagrams for the three substitutional subsurface doping sites $(\text{sub } 3)_s$, $(\text{sub } 3)_m$, and $(\text{sub } 3)_i$ for a $Si_{40}MnH_{60}$ NC. The gray regions correspond to conduction and valence states of the bare (undoped) Si NCs. The black lines represent the energy levels of the doped Si NCs. The degeneracy of the TM $3d$ states (e_g—blue and t_{2g}—red) is illustrated by open (empty) and filled (occupied) circles. Results in (a) GGA and (b) GGA+U (U=3 eV) are presented. The horizontal dotted line defines the Fermi level. Majority-spin (left) and minority-spin (right) channels are shown.

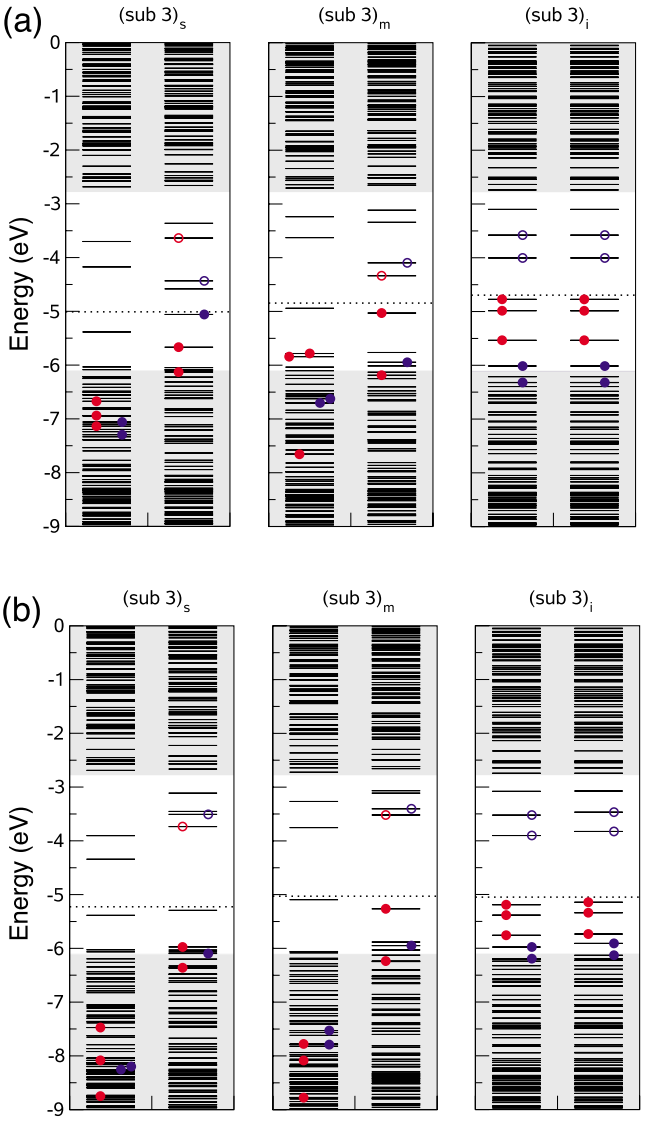

FIG. 10. (Color online) As in Fig. 9 but Fe instead of Mn.

spin (Fe) character in GGA and GGA+U, the $(\text{sub } 3)_i$ geometry corresponds to the low-spin phase in both XC approaches and for both TM atoms, Mn and Fe. The reason for this spin-phase transition is the significant change in the structural arrangement (see Fig. 4) which is reflected in the electronic structure. While the doping sites $(\text{sub } 3)_s$ and $(\text{sub } 3)_m$ have qualitatively similar electronic properties, the doping site $(\text{sub } 3)_i$ differs considerably. In particular, the occupied Si sp^3-like state below the Fermi level in the majority-spin channel is shifted to higher energies which causes a spin flip and, hence, leads to the observed spin-phase transition. Consequently, one has to state a significant sensibility of the electronic and magnetic properties of the NCs with subsurface doping sites on the actual geometry, doping species, and the strength of the electronic correlation.

D. Dependence of the impurity states on the NC size

In order to discuss the Si NC size dependence of the TM impurity states we have plotted the energy-level diagrams for the most stable doping sites $(\text{sub } N-1)_m$ and $(\text{int } N-1)^+$ in Fig. 11. The most striking feature is the well-known quantum confinement effect on the Si NC states, i.e, we observe increasing HONO-LUNO gap values between empty and occupied Si sp^3-orbital-derived bonding and antibonding states with decreasing quantum-dot size. The fundamental gaps are in agreement with the well-known results E_g=5.64 (N_{Si}=5), 4.17 (N_{Si}=17), 3.22 (N_{Si}=41), 2.78 (N_{Si}=83), and 2.29 eV (N_{Si}=147).[24,25] In Mn-doped Si NCs (with more than three Si shells) gaps appear between occupied and empty defect levels in both the majority-spin and minority-spin channels.

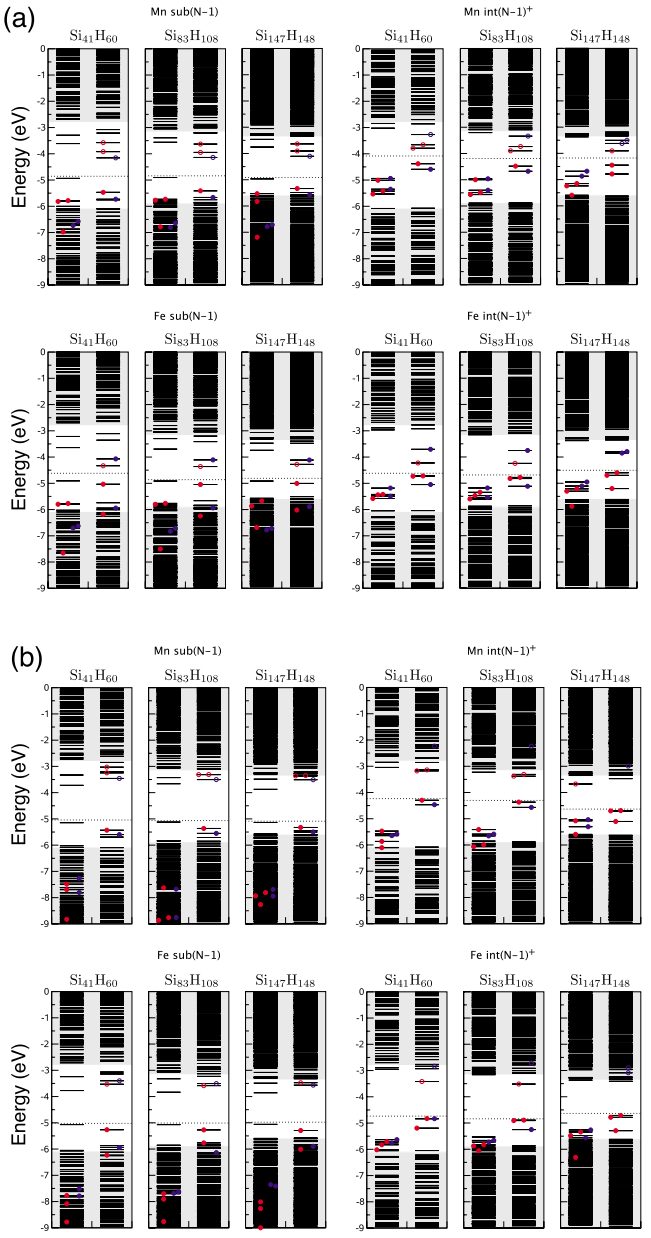

FIG. 11. (Color online) Energy-level diagrams of TM-doped Si NCs within (a) GGA and (b)GGA+U. The gray regions correspond to conduction and valence states of the bare (undoped) Si NCs. The horizontal black lines represent the energy levels of the doped Si NCs. The degeneracy of the TM 3d states (e_g—blue and t_{2g}—red) is illustrated by open (empty) and filled (occupied) circles. The Fermi level is indicated as horizontal dotted line. The vacuum level is used as energy zero.

In the interstitial case the gap is given by t_{2g}-t_{2g}-derived states in the minority-spin channel while for substitutional impurities gaps of similar magnitude occur in both spin channels. One important difference with respect to the electronic structure between the substitutional and interstitial doping sites is the different position of the t_{2g}-bonding combinations with mainly Mn 3d character. They are localized close to the highest Si NC states and form strong resonances with the Si states at substitutional doping sites. On the other hand, at interstitial doping sites the highest bonding Mn 3d states are localized below the Fermi level. Due to the higher position (about 0.9 eV) of the Fermi level in this case they lie clearly inside the fundamental band-gap region and contain a much smaller fraction of Si-like states. In the GGA case the antibonding t_{2g} states are localized 0.8–1.2 eV (0.3–0.7 eV) above the Fermi level in substitutional (interstitial) cases. Consequently in Mn-doped Si NCs with substitutional doping sites we obtain ~0.5 eV larger band gaps compared to the interstitial doping sites. Apart from the shift of the antibonding TM 3d states to higher energies and hence an increased gap value the same holds for GGA+U calculations. Only in the case of a (int 5)$^+$ $Si_{146}MnH_{148}$ NC larger deviations appear. In this case the magnetic moment changes within the GGA+U approach to the low-spin phase $\mu_{tot}=1\mu_B$ (see Table II). The reason for this different behavior is the formation of bonds to neighboring surface hydrogen atoms.

For Fe-doped Si NCs the energy-level picture changes slightly. Despite the even number of electrons the majority-spin and minority-spin channels show nonsymmetric electronic structures. They are close to the situation of Mn-doped Si NCs. The difference is essentially a shift of one antibonding t_{2g} state of the minority-spin channel below the Fermi level. The gaps between the impurity states are formed in the same manner as in the Mn case. However, especially in the GGA treatment of the substitutional doping sites the t_{2g} states of the minority-spin channel are lower in energy so that we obtain fundamental gaps between impurity states of ~0.5 eV GGA or ~1 eV (GGA+U) at both substitutional and interstitial doping sites. Similar to the Mn-doped NCs, for all Fe-doped NCs with more than three Si shells and subsurface doping sites, we observe a nonvanishing magnetic moment. Here the mediate-spin phase, i.e., a magnetic moment of $2\mu_B$ is preferred (see Table II). The equivalence of both systems, Mn- and Fe-doped Si NCs, shows that the Fe impurities behave very much like Mn^- impurities. Only for the (int 5)$^+$ impurity of the $Si_{146}FeH_{148}$ NC this picture fails. In contrast to the Mn-doped case no spin flip occurs, which means the GGA and GGA+U yield the same total magnetic moment of $2\mu_B$.

In both cases, Mn- and Fe-doped Si NCs, the energetic positions of the impurity states with respect to the Fermi level are more or less independent of the NC size, which is a result of the strong localization of the TM 3d-derived states at the impurity sites.

IV. SUMMARY

The incorporation of Mn and Fe impurities in silicon nanocrystals at substitutional and interstitial doping sites has been studied in the framework of the *ab initio* density-functional theory and a semilocal approximation for exchange and correlation as well as adding a Hubbard-type on-site Coloumb repulsion U to describe the stronger electron correlation for the more localized 3d states. In this way it was possible to study directly the influence of strong electron correlation on a nanoscale. In particular, its influence on the electronic and magnetic properties of Si NCs with substitutional and interstitial TM doping sites have been studied.

TABLE II. Total magnetic moment μ_{tot} in units of μ_B of single-doped Si NCs of different sizes. Only results for the energetically most favored substitutional or interstitial sites are listed.

Number of shells N		3	4	5	6
Mn(GGA)	sub $(N-1)$	3	3	3	3
	int $(N-1)^+$		3	3	3
Mn(GGA+U)	sub $(N-1)$	3	3	3	3
	int $(N-1)^+$		3	3	1
Fe(GGA)	sub $(N-1)$	2	2	2	2
	int $(N-1)^+$		2	2	2
Fe(GGA+U)	sub $(N-1)$	2	2	2	2
	int $(N-1)^+$		2	2	2

The most stable doping sites depend significantly on the size of the nanocrystal and the preparation conditions. Under Si-rich conditions, for example, the interstitial doping sites below the rectangular {001} facets are preferred. Under Si-poor conditions on the other hand doping sites close to the NC surface are more energetically favorable. In addition, we have shown a clear evidence of self-purification effects in small TM-doped Si NCs.

The resulting electronic properties depend on the size of the Si NCs, the impurity site, and the chemical nature of TM atoms. While all Fe-doped NCs exhibit a insulating character in some very small Mn-doped systems a half-metallic character could be observed. There are several impurity-induced levels in the fundamental gap mainly derived from TM 3*d* states with e_g and t_{2g} symmetry. Beside the nonbonding e_g states also bonding (i.e., TM 3*d* dominated) and antibonding (i.e., Si sp^3 dominated) combinations with t_{2g} contributions of the four neighboring Si sp^3 orbitals occur. For impurity sites outside the NC center, of course the T_d symmetry is disturbed and the degeneracy of the e_g and t_{2g} levels is partly or fully lifted. The total magnetic moment of the TM-doped Si NCs can easily be obtained by counting the electrons on occupied levels within the two spin channels. Therefore, the total magnetic moment μ_{tot} of the doped Si NC depend on the number and the relative position of the TM impurity-induced states in the minority-spin and majority-spin channels. For Mn-doped NCs μ_{tot} can be 1 or $3\mu_B$ while for Fe-doped NCs values of 0 or $2\mu_B$ have been observed. The results are in agreement with those of the Ludwig-Woodbury model developed for TM doping of bulk Si crystals. While for bulk Si many studies are available concerning the incorporation of TM atoms, for nanostructured Si exist only few studies dealing with Si nanowires.[17] The sometimes observed half-metallic character of these structures[18] is in contrast to the results for TM-doped Si NCs.

Of special importance is the large influence of the treatment of strong electron-correlation effects. That means the electronic and magnetic properties change considerable by going over from a semilocal GGA approach of XC to a GGA+U treatment, where the spin-dependent correlation of electrons in the localized TM 3*d* states is derived by a Coulomb integral U.

ACKNOWLEDGMENTS

The work was financially supported through the Fonds zur Förderung der Wissenschaftlichen Forschung (Austria) in the framework of SFB25, Nanostrukturen für Infrarot-Photonik (IR-ON), the Deutsche Forschungsgemeinschaft (Project No. Be1346/20-1), and the EU I3 ETSF project (Grant No. 211956). Grants of computer time from the Höchstleistungsrechenzentrum Stuttgart are gratefully acknowledged.

*roman@ifto.physik.uni-jena.de

†Permanent adress: Energieforschungszentrum Niedersachsen, Technische Universität Clausthal, Am Stollen 19, 38640 Goslar, Germany.

[1] H. Ohno, Science **281**, 951 (1998).

[2] I. Žutić and J. Fabian, Nature (London) **447**, 268 (2007).

[3] K. Sato and H. Katayama-Yoshida, Semicond. Sci. Technol. **17**, 367 (2002).

[4] D. Awschalom and J. Kikkawa, Nature (London) **397**, 139 (1999).

[5] D. Awschalom and J. Kikkawa, Phys. Today **52** (6), 33 (1999).

[6] G. Burkard, D. Loss, and D. P. DiVincenzo, Phys. Rev. B **59**, 2070 (1999).

[7] F. Beeler, O. K. Andersen, and M. Scheffler, Phys. Rev. B **41**, 1603 (1990).

[8] A. Zunger and U. Lindefelt, Phys. Rev. B **27**, 1191 (1983).

[9] H. Katayama-Yoshida and A. Zunger, Phys. Rev. B **31**, 8317 (1985).

[10] Z. Z. Zhang, B. Partoens, Kai Chang, and F. M. Peeters, Phys. Rev. B **77**, 155201 (2008).

[11] S. C. Erwin, L. Zu, M. I. Haftel, A. L. Efros, T. A. Kennedy, and D. J. Norris, Nature (London) **436**, 91 (2005).

[12] X. Huang, A. Makmal, J. R. Chelikowsky, and L. Kronik, Phys. Rev. Lett. **94**, 236801 (2005).

[13] G. M. Dalpian and J. R. Chelikowsky, Phys. Rev. Lett. **96**, 226802 (2006).

[14] Y. Léger, L. Besombes, L. Maingault, J. Fernández-Rossier, D. Ferrand, and H. Mariette, Phys. Status Solidi B **243**, 3912

(2006).
[15] A. Nag and D. Sarna, J. Phys. Chem. C **111**, 13641 (2007).
[16] J. T. Arantes, G. M. Dalpian, and A. Fazzio, Phys. Rev. B **78**, 045402 (2008).
[17] H. Wu, P. Kratzer, and M. Scheffler, Phys. Rev. Lett. **98**, 117202 (2007).
[18] W. H. Wu, C. J. Tsai, and L. J. Chen, Appl. Phys. Lett. **90**, 043121 (2007).
[19] F. Kuewen, R. Leitsmann, C. Roedl, C. Panse, and F. Bechstedt (unpublished).
[20] H. Katayama-Yoshida and A. Zunger, Phys. Rev. Lett. **53**, 1256 (1984).
[21] H. Katayama-Yoshida and A. Zunger, Phys. Rev. Lett. **55**, 1618 (1985).
[22] V. I. Anisimov, J. Zaanen, and O. K. Andersen, Phys. Rev. B **44**, 943 (1991).
[23] M. C. Payne, M. P. Teter, D. C. Allan, T. A. Arias, and J. D. Joannopoulos, Rev. Mod. Phys. **64**, 1045 (1992).
[24] L. E. Ramos, J. Furthmüller, and F. Bechstedt, Phys. Rev. B **72**, 045351 (2005).
[25] L. E. Ramos, H.-C. Weissker, J. Furthmüller, and F. Bechstedt, Phys. Status Solidi B **15**, 3053 (2005).
[26] G. Kresse and J. Furthmüller, Comput. Mater. Sci. **6**, 15 (1996).
[27] G. Kresse and D. Joubert, Phys. Rev. B **59**, 1758 (1999).
[28] J. P. Perdew, *Electronic Structure of Solids '91* (Akademie Verlag, Berlin, 1991), p. 11.
[29] J. P. Perdew and Y. Wang, Phys. Rev. B **45**, 13244 (1992).
[30] U. von Barth and L. Hedin, J. Phys. C **5**, 1629 (1972).
[31] F. Kuwen, R. Leitsmann, and F. Bechstedt, Phys. Rev. B **80**, 045203 (2009).
[32] A. Stroppa, S. Picozzi, A. Continenza, and A. J. Freeman, Phys. Rev. B **68**, 155203 (2003).
[33] I. Appelbaum, B. Huang, and D. Monsma, Nature (London) **447**, 295 (2007).
[34] W. G. Aulbur, L. Jönsson, and J. W. Wilkins, Solid State Phys., Adv. Res. Appl. **54**, 1 (2000).
[35] V. I. Anisimov and O. Gunnarsson, Phys. Rev. B **43**, 7570 (1991).
[36] S. L. Dudarev, G. A. Botton, S. Y. Savrasov, C. J. Humphreys, and A. P. Sutton, Phys. Rev. B **57**, 1505 (1998).
[37] C. Rödl, F. Fuchs, J. Furthmuller, and F. Bechstedt, Phys. Rev. B **77**, 184408 (2008).
[38] The cage spanned by eight Si atoms within zinc-blende structure.
[39] G. Cantele, E. Degoli, E. Luppi, R. Magri, D. Ninno, G. Iadonisi, and S. Ossicini, Phys. Rev. B **72**, 113303 (2005).
[40] H. Peelaers, B. Partoens, and F. M. Peeters, Nano Lett. **6**, 2781 (2006).
[41] L. Ramos, E. Degoli, G. Cantele, S. Ossicini, D. Ninno, J. Furthmüller, and F. Bechstedt, J. Phys.: Condens. Matter **19**, 466211 (2007).
[42] F. Iori, S. Ossicini, E. Degoli, E. Luppi, R. Poli, R. Magri, G. Cantele, F. Trani, and D. Ninno, Phys. Status Solidi A **204**, 1312 (2007).
[43] L. E. Ramos, J. Furthmüller, and F. Bechstedt, Phys. Rev. B **70**, 033311 (2004).
[44] G. W. Ludwig and H. H. Woodbury, *Solid State Physics* (Academic, New York, 1962), Vol. 13.